INTERNATIONAL SOCIETY
FOR ROCK MECHANICS

SOCIETE INTERNATIONALE
DE MECANIQUE DES ROCHES

INTERNATIONALE GESELLSCHAFT
FÜR FELSMECHANIK

International Congress on
Rock Mechanics

Congrès International
de Mécanique des Roches

Internationaler Kongress
über Felsmechanik

PROCEEDINGS / COMPTES-RENDUS / BERICHTE

VOLUME / TOME / BAND 3

Editor / Editeur / Herausgeber
T.FUJII

OFFPRINT/SONDERDRUCK/TIRE-A-PART

Tokyo / Japan / 1995

Elastic interface wave propagation along a fracture

Propagation de l'onde d'interface élastique le long d'une fracture
Elastische Interfacewellenausbreitung entlang einer Bruchfuge

KURT T. NIHEI, BOLIANG GU & LARRY R. MYER, Lawrence Berkeley Laboratory, Calif., USA
LAURA J. PYRAK-NOLTE, University of Notre Dame, Ind., USA
NEVILLE G.W. COOK, University of California, Berkeley, USA

ABSTRACT: Fractures in rock can serve as mechanical waveguides for elastic interface waves. Because the energy of the interface wave is confined mainly to the fracture, these waves primarily sample the mechanical properties of the fracture and, therefore, should prove useful for remotely determining fracture properties. Plane wave analysis of a fracture embedded in an elastic medium predicted two distinct fracture interface waves with mathematical forms similar to the classic free-surface Rayleigh wave equation, indicating that these interface waves are generalized Rayleigh+ interface waves. Analysis of the interface wave equations revealed that both waves are dispersive and that each wave depends on either a normal or shear dimensionless fracture stiffness. The predicted interface waves were observed in both numerical simulations and laboratory tests. Numerical simulations also produced a compressional interface wave that is not predicted by the plane wave theory. The results of this study demonstrate how interface waves can be excited and detected on a single fracture and how measured interface wave velocities can be used to determine the fracture stiffnesses.

RESUME: Les fractures dans un rocher peuvent servir comme guides d'ondes pour les ondes élastiques d'interface. Puisque l'énergie d'un onde d'interface est attribué en majorité à la fracture, ces ondes illustrent les caractéristiques méchanique de la fracture et par conséquense devraient se prouver utiles pour determiner les caractéristiques d'une fracture à grande distance. Une analyse simple des ondes d'une fracture se trouvant dans un milieu élastique prévoit deux ondes de fracture d'interface differents avec des formes mathématiques similaires à l'equation classique d'ondes de la surface libre de Rayleigh, indiquant que ces ondes d'interface sont les ondes d'interface généralisées de Rayleigh. Les analyses des équations d'ondes d'interface démontrent que les deux ondes sont dispersives et que chaque onde dépend de la solidite de la fracture normale ou partagé sans dimension. Les ondes d'interface prévues ont été observeés également dans les simulations numériques et dans les test en laboratoire. Les simulations numériques ont produit également une onde de compression d'interface qui n'est pas prévue par la théorie simple des ondes. Les résultats de cette étude démontrent comment les ondes d'interface peuvent être exciteés et detecteés sur une fracture simple et comment les vitesses mesurés des onde d'interface peut étre utilisées pour déterminer la solidité de la fracture.

ZUSAMMENFASSUNG: Gesteinsrisse können als mechnische Kanäle für elastische Grenzwellen dienen. Die Energie der Grenzwelle ist hauptsächlich im Bereich des Risses konzentriert und wird somit von dessen mechanischen Eigenschaften beeinflußt. Es besteht daher die Möglickkeit, die Grenzwellen zur Bestimmung von Rissparametern zu benutzen. Die Theory der ebenen Wellen, angewandt auf einen in einem elastische Medium eingebetten Riß, deutet auf zwei unterschiedliche Riß-Grenzwellen hin, deren mathematische Form der klassischen Rayleighwelle an der freien Oberfläche ähnelt. Dies deutet darauf hin, daß die erzeugte Grenzwellen generalisierte Rayleighwellen darstellen. Die Analyse der Wellen zeigt, daß beide dipersiven Character aufweisen, und Funktionen der normalen und Scher Steifigkeit des Risses sind. Die von der Theorie beschriebenen Grenzwellen sind in numersiche Modellierungen und Laborversuchen nachgewiesen worden. Gleizeitig erzeugen die numerischen Untersuchungen eine Kompressions-Grenzwelle, die nicht von der Theorie ebener Wellen vorhergesagt wird. Die vorgestellten Untersuchungen zeigen, daß Grenzwellen an Rissen erzeugt und nachgewiesen werden können, und daß die Rißsteifigkeit von der Geschwindigkeit der Grenzwellen abgeleitet werden kann.

1 INTRODUCTION

One of the most important characteristics of rocks is that they are discontinuous on all scales from microcracks to faults. These discontinuities make rock weak in tension despite its considerable compressive strength. They also make rock capable of storing and transporting fluids. The mechanical and hydraulic properties of these discontinuities are of the utmost importance in relation to the production of energy resources, such as hydrocarbons and geothermal energy, the isolation of nuclear and other wastes, and the remediation of contaminated sites. Faced with the responsibility of assessing the continued integrity and stability of underground waste repositories, excavations and geostructures in fractured rock and enhancing oil and gas production in hydraulically and naturally fractured reservoirs, it is essential that geophysical techniques be developed for locating and characterizing the mechanical and hydraulic properties of fractures.

It has recently been discovered that fractures possess distinct seismic properties that may prove useful for remotely evaluating the mechanical properties of fractured rock. The compliant nature of fractures in rock produces a variety of potentially diagnostic effects on the displacements and velocities of elastic waves propagating across or along fractures. Field and laboratory tests have established that an elastic wave incident upon a fracture is partially transmitted and reflected by a process which partitions low frequencies into the transmitted wave and high frequencies into the reflected wave (Myer and Majer, 1984; Pyrak-Nolte et al., 1990a,b; Suárez-Rivera, 1992). In addition, recent laboratory measurements have confirmed the existence of two dispersive interface waves that propagate along the fracture (Pyrak-Nolte et al., 1992), both of which are predicted by the theory of Pyrak-Nolte and Cook (1987). Fracture interface waves primarily probe the mechanical properties of a fracture and, therefore, offer unique prospects for directly measuring fracture stiffnesses. This paper describes the properties of elastic interface waves on single fractures using a combination of plane wave analysis, numerical simulation and laboratory measurements, and discusses techniques for generating and detecting fracture interface waves.

2 MECHANICAL PROPERTIES OF FRACTURES IN ROCK

At the microscale, fractures in rock appear as two surfaces of irregular topography which intersect to form void spaces and asperities of contact. The presence of the void spaces within a planar fracture collectively define a thin, compliant zone with effective normal and shear stiffnesses that can range from near zero for open fractures, to values in excess of 10^{13} Pa/m for fractures which are cemented or subjected to high compressive stresses (Pyrak-Nolte, 1988). A fracture loaded in shear or compression typically exhibits a highly nonlinear stress-displacement relationship (Fig.1) resulting from deformation of the asperities, the number and distribution of which changes with load (Cook, 1992). Hysteresis may also be present in the stress-displacement curve (Fig.1), indicating the presence of inelastic deformation of the asperities of contact and frictional sliding between contacts oriented at some angle relative to the applied stress (Goodman, 1976; Bandis et al., 1983; Barton et al., 1985).

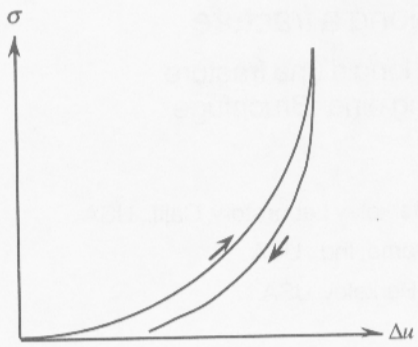

Figure 1. Schematic illustration of the stress-displacement characteristics of a fracture subjected to normal compression.

For most seismic applications in the field and laboratory, it is generally assumed that the strains produced by an elastic wave incident upon a fracture are too small to cause relative displacements across the fracture sufficient to exercise fracture nonlinearity and hysteresis. For these applications, the constitutive properties of the fracture are well approximated by linear elastic relationships between the normal and shear tractions applied to the fracture and the resulting relative normal and shear displacements across and along the fracture,

$$t_n = \kappa_n \Delta u_n$$
$$t_t = \kappa_t \Delta u_t \ , \tag{1}$$

where t_n and t_t are the normal and shear tractions, κ_n and κ_t are the normal and shear fracture stiffnesses, and $\Delta u_n = [u_n^b - u_n^a]$ and $\Delta u_t = [u_t^b - u_t^a]$ are the displacement-discontinuities describing the relative closure and shear between the upper (denoted by the superscript *a*) and lower (denoted by the superscript *b*) fracture surfaces. Newton's Third Law requires that the tractions across the fracture be continuous as in the case of a continuous medium,

$$t_n^b = -t_n^a = t_n \ .$$
$$t_t^b = -t_t^a = t_t \ . \tag{2}$$

Numerical studies (Angel & Achenbach, 1985) have demonstrated that the dynamic fracture stiffness is independent of wave frequency provided that the wavelength is greater than the spacing between the asperities of contact, a condition which is valid for most fractures provided that frequencies are kept below 1 MHz. Under these conditions, the fracture stiffnesses appearing in Eq.(1) are well approximated by their static values which can be computed from the tangent to the unloading portions of the stress-displacement curves where friction is locked-up (Cook & Hodgson, 1965; Walsh, 1965; Stoll, 1989). Eq.(1) and (2) form a simple model for the linear elastic properties of a nonwelded contact between two media that has also found application in ultrasonic nondestructive testing of welds and adhesive bonds (Nagy et al., 1990; Rokhlin & Wang, 1991). In the remainder of this paper, Eq.(1) and (2) will be referred to as the *displacement-discontinuity* model of a nonwelded interface (Pyrak-Nolte, 1988), but it should be noted that a variety of other terms have been used to describe the same constitutive model, including the *incomplete interface* model (Kendall & Tabor, 1971), the *slip interface* model (Schoenberg, 1980), and the *imperfect interface* model (Rokhlin & Wang, 1991). The displacement-discontinuity model is a generalization of the classic boundary conditions encountered in most seismology problems in the sense that it degenerates to the boundary conditions for a welded interface as $\kappa_n, \kappa_t \to \infty$ and for a traction-free interface as $\kappa_n, \kappa_t \to 0$.

3 FRACTURE INTERFACE WAVES

Interface waves represent a class of elastic waves that propagate along the boundary between two media. *Trapped* interface waves are localized within a zone that may extend only a few wavelengths away from the fracture, allowing these waves to propagate large distances while suffering little reduction in amplitude. *Leaky* interface waves continuously radiate elastic body waves as they propagate along the fracture and, consequently, suffer from an increasing loss of amplitude with increasing propagation distance along the fracture. Since interface waves primarily sample the mechanical properties of the fracture as they propagate away from the source to the receiver, these waves may contain diagnostic information on the mechanical properties of the fracture. This section presents plane wave theory, numerical boundary element simulations, and laboratory modeling of interface waves propagating along the surface of a single fracture. The results of this analysis demonstrate: (1) how measured velocities and particle displacements can be used to determine the normal and shear stiffnesses of a fracture, (2) the existence of other types of fracture interface waves, and (3) techniques for generating and detecting interface waves.

3.1 *Plane Wave Analysis*

The displacements for an inhomogeneous plane wave propagating along the fracture with an amplitude that decays exponentially with distance away from the fracture can be expressed as (Pyrak-Nolte & Cook, 1987; Gu et al., 1995)

$$u_x^a = \omega \left[ic^{-1} A_1 e^{-p\omega z} + q B_1 e^{-q\omega z} \right] e^{i\omega(x/c - t)}$$
$$u_z^a = \omega \left[-p A_1 e^{-p\omega z} + ic^{-1} B_1 e^{-q\omega z} \right] e^{i\omega(x/c - t)} \tag{3}$$

for the upper medium, denoted by the superscript *a*, and

$$u_x^b = \omega \left[ic^{-1} A_2 e^{+p\omega z} - q B_2 e^{+q\omega z} \right] e^{i\omega(x/c - t)}$$
$$u_z^b = \omega \left[p A_2 e^{+p\omega z} + ic^{-1} B_2 e^{+q\omega z} \right] e^{i\omega(x/c - t)} \tag{4}$$

for the lower medium, denoted by the superscript *b*., where ω is the angular frequency, t is time, A_1, A_2, B_1 *and* B_2 are undetermined constants, c is the phase velocity of the inhomogeneous wave, and p and q are wavenumbers defined as

$$p = [c^{-2} - c_p^{-2}]^{1/2}$$
$$q = [c^{-2} - c_s^{-2}]^{1/2} \tag{5}$$

where c_p and c_s are the P- and S-wave velocities, respectively. Tractions in the upper and lower media obtained by substituting Eq.(3) and (4) into Hooke's Law are

$$t_x^a = \omega^2 \left[-2ic^{-1} p\mu A_1 e^{-p\omega z} - \mu M B_1 e^{-q\omega z} \right] e^{i\omega(x/c - t)}$$
$$t_z^a = \omega^2 \left[\left(L p^2 - \lambda c^{-2} \right) A_1 e^{-p\omega z} - 2i\mu c^{-1} q B_1 e^{-q\omega z} \right] e^{i\omega(x/c - t)}$$
$$t_x^b = -\omega^2 \left[2ic^{-1} p\mu A_2 e^{+p\omega z} - \mu M B_2 e^{+q\omega z} \right] e^{i\omega(x/c - t)} \tag{6}$$
$$t_z^b = -\omega^2 \left[\left(L p^2 - \lambda c^{-2} \right) A_2 e^{+p\omega z} + 2i\mu c^{-1} q B_2 e^{+q\omega z} \right] e^{i\omega(x/c - t)}$$

where λ and μ are the Lame's constants, $L = (\lambda + 2\mu)$, and $M = (c^{-2} + p^2)$.

Substituting Eq.(3), (4) and (6) into the displacement-discontinuity boundary conditions given in Eq.(1) and (2) yields a system of four homogeneous, linear equations in the four constants A_1, A_2, B_1 and B_2 ,

$$ic^{-1}(\kappa_x + 2\mu\omega p) A_1 + (q\kappa_x + \mu\omega N) B_1 - ic^{-1} \kappa_x A_2 + q\kappa_x B_2 = 0$$
$$(\omega Q - p\kappa_z) A_1 + ic^{-1}(\kappa_z + 2\mu\omega q) B_1 - p\kappa_z A_2 - ic^{-1} \kappa_z B_2 = 0$$
$$-2ic^{-1}\mu p A_1 - \mu N B_1 - 2ic^{-1}\mu p A_2 + \mu N B_2 = 0 \tag{7}$$
$$-Q A_1 - 2ic^{-1}\mu q B_1 + Q A_2 - 2ic^{-1}\mu q B_2 = 0$$

where $N = (c^{-2} + q^2)$ and $Q = (\lambda c^{-2} - L p^2)$.
The condition for the existence of a non-trivial solution of Eq.(7) is that the determinant of the coefficients of A_1, A_2, B_1 and B_2 vanish.

Examination of the terms in the last two equations of Eq.(7) reveals that there are two possible solutions corresponding to:

1. $B_2 = -B_1$, $A_2 = A_1$ (8)
2. $B_2 = B_1$, $A_2 = -A_1$. (9)

Upon substitution of Eq.(8) into Eq.(3) and (4), it becomes apparent that case 1 produces extensional wavemotion characterized by horizontal displacements that are symmetric about the fracture plane and that case 2 produces flexural wavemotion characterized by horizontal displacements that are antisymmetric about the fracture (Fig.7).

Substituting Eq.(8) into Eq.(7) yields the dispersion equation for the *symmetric* interface wave (Fig.7),

$$4\frac{1}{\theta^2}\sqrt{\frac{1}{\theta^2}-\frac{1}{\vartheta^2}}\left(\frac{\kappa_z}{\omega z_s}+\sqrt{\frac{1}{\theta^2}-1}\right) -\left(1-2\frac{1}{\theta^2}\right)\left[\left(1-2\frac{1}{\theta^2}\right)-2\sqrt{\frac{1}{\theta^2}-\frac{1}{\vartheta^2}}\frac{\kappa_z}{\omega z_s}\right]=0 \quad , \tag{10}$$

where $\theta = c/c_s$, $\vartheta = c_p/c_s$, and $z_s = \rho c_s$ is the S-wave impedance. Similarly, substitution of Eq.(9) into Eq.(7) yields the dispersion equation for the *antisymmetric* interface wave (Fig.7),

$$4\frac{1}{\theta^2}\sqrt{\frac{1}{\theta^2}-1}\left(\frac{\kappa_x}{\omega z_s}+\sqrt{\frac{1}{\theta^2}-\frac{1}{\vartheta^2}}\right) -\left(1-2\frac{1}{\theta^2}\right)\left[\left(1-2\frac{1}{\theta^2}\right)-2\sqrt{\frac{1}{\theta^2}-1}\frac{\kappa_x}{\omega z_s}\right]=0 \quad . \tag{11}$$

The symmetric and antisymmetric interface waves described by Eq.(10) and (11) are *generalized Rayleigh waves*. That is, when the dimensionless fracture stiffnesses $\kappa_z/(\omega z_s)$ and $\kappa_x/(\omega z_s)$ are set to zero, both Eq.(10) and (11) degenerate to the Rayleigh equation for surface waves on a traction-free surface (Aki & Richards, 1980, p.161). However, when the dimensionless fracture stiffnesses are finite, Eq.(10) and (11), unlike the Rayleigh equation, contain wave frequency. Therefore, the interface waves propagating along a fracture with finite dimensionless stiffness are dispersive. Note that κ_z and κ_x appear in Eq.(10) and (11), respectively. This indicates that the symmetric interface wave results from the normal coupling between the surfaces of the fracture and the antisymmetric interface wave, from the tangential coupling. If the rock properties are different on the two sides of the fracture, then the two interface waves become *generalized Stoneley waves* that propagate along the fracture only for a specific range of shear moduli ratios and wave frequencies (Pyrak-Nolte & Cook, 1987).

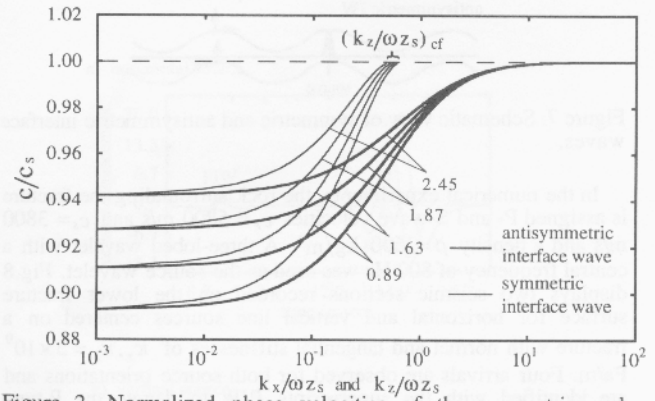

Figure 2. Normalized phase velocities of the symmetric and antisymmetric interface waves as a function of the dimensionless fracture stiffnesses for a range of c_p/c_s ratios: 0.89, 1.63, 1.87 and 2.45 (corresponding to Poisson's ratios of 0.1, 0.2, 0.3 and 0.4, respectively). The numbers labeled on the curves are the c_p/c_s values, and $(\kappa_z/\omega z_s)_{cf}$ is the dimensionless cut-off stiffness above which the trapped symmetric interface wave ceases to exist.

The roots of the nonlinear dispersion Eq.(10) and (11) are the normalized phase velocities, c/c_S, of the two interface waves for given dimensionless fracture stiffnesses $\kappa_z/\omega z_s$ and $\kappa_x/\omega z_s$. Fig.2 displays c/c_S for a range of c_p/c_s ratios. As $\kappa_z/\omega z_s$ and $\kappa_x/\omega z_s$ increase, the phase velocities of the two interface waves increase from the Rayleigh wave velocity to the shear wave velocity, with the symmetric interface wave propagating faster than the antisymmetric interface wave. Examination of the dimensionless fracture stiffness term reveals that decreasing ω and z_s has the same effect as increasing κ_z and κ_x. Thus, as z_s is decreased for given values of κ_z, κ_x and ω, the fracture is effectively stiffened even though the fracture stiffnesses are not increased. Equivalently, as the frequency of the wave is reduced for given values of κ_z, κ_x and z_s, the fracture is also effectively stiffened. The curves in Fig.2 show that an increase in the Poisson's ratio of the rock surrounding the fracture results in an increase in the phase velocities of the interface waves relative to the S-wave velocity of the rock. This occurs because as the Poisson's ratio is increased (i.e., as the dilatation of the rock surrounding the fracture is increased), the fracture becomes effectively stiffer even though the fracture stiffnesses are not increased. This effective stiffening of the fracture results in higher interface wave phase velocities relative to the S-wave velocity. This behavior is consistent with that of a free-surface Rayleigh wave for which there is an observed increase in the velocity of the Rayleigh wave with increasing Poisson's ratio.

When the solution range for the roots of Eq.(10) and (11) is extended to the complex domain, complex roots of Equation (10) are obtained for the symmetric interface wave for $\kappa_z/\omega z_s > (\kappa_z/\omega z_s)_{cf}$ (Fig.3). These roots correspond to a symmetric interface wave with a phase velocity between c_s and c_p. Since the phase velocity is complex in this range, the symmetric interface wave suffers a loss in amplitude as it propagates along the interface as a result of energy radiation into the rock surrounding the fracture. Thus, for $\kappa_z/\omega z_s > (\kappa_z/\omega z_s)_{cf}$, the symmetric interface wave becomes a leaky wave which propagates with a phase velocity between the S- and P-wave velocities, as shown in Fig.3. Note that no dimensionless cut-off stiffness and complex roots of Eq.(11) were found, indicating that the antisymmetric interface wave exists for all possible dimensionless stiffness values as a trapped interface wave.

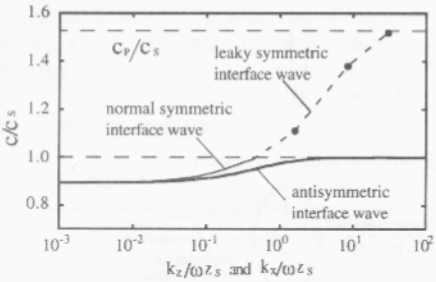

Figure 3. Normalized phase velocities of the symmetric and antisymmetric interface waves as a function of the dimensionless fracture stiffness for c_p/c_s=1.53.

An explicit equation for the dimensionless fracture stiffness $(\kappa_z/\omega z_s)_{cf}$ which defines the boundary between the normal (i.e., trapped) and leaky domains of the symmetric interface wave can be found by setting $\theta = 1$ in Eq.(10),

$$\left(\frac{\kappa_z}{\omega z_s}\right)_{cf} = 2\sqrt{2(1-\upsilon)} \quad . \tag{12}$$

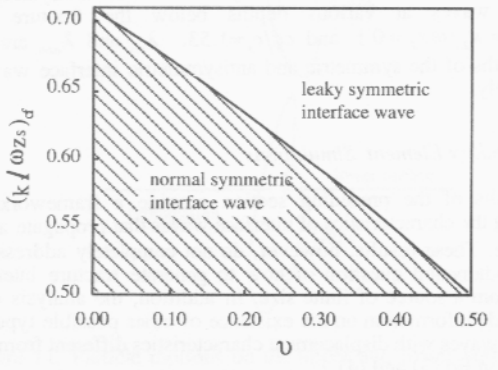

Figure 4. Dimensionless cut-off stiffness of the symmetric interface wave as a function of the Poisson's ratio.

Eq.(12) is the dimensionless cut-off stiffness of the symmetric interface wave. The dimensionless cut-off stiffness is depicted as a function of Poisson's ratio in Fig.4.

Particle motions of the two interface waves, computed from Eq.(3) and (4), for are plotted in Fig.5. The particle motions of both the symmetric and antisymmetric interface waves, like those of the free-surface Rayleigh wave, are retrograde near the fracture and reverse to prograde at a depth of approximately 0.2 wavelengths away from the fracture. An analysis of Eq.(1) and (2) for $\kappa_x/\omega z_s \to \infty$ (Gu et al., 1995) revealed that the particle motion of the antisymmetric interface wave approaches that of an S-wave propagating parallel to the fracture, which is consistent with its phase velocity approaching the S-wave velocity as $\kappa_x/\omega z_s \to \infty$, as shown in Fig.2 and 3. A similar analysis of the particle motion of the symmetric interface wave as $\kappa_z/\omega z_s \to \infty$ revealed that the displacement approaches that of a P-wave propagating parallel to the fracture, which is consistent with the phase velocity of the symmetric interface wave approaching the P-wave velocity, as observed in Fig.2 and 3.

a) a symmetric interface wave

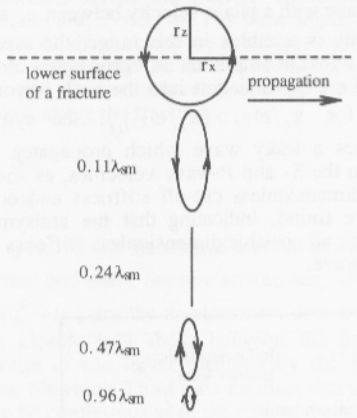

b) an antisymmetric interface wave

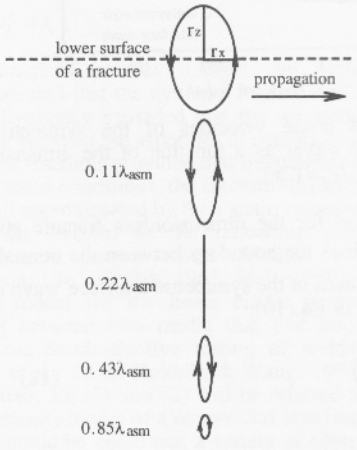

Figure 5. Particle motion of the symmetric and antisymmetric interface waves at various depths below the fracture for $\kappa_x/\omega z_s = \kappa_z/\omega z_s = 0.1$ and c_p/c_s=1.53. λ_{sm} and λ_{asm} are the wavelengths of the symmetric and antisymmetric interface waves, respectively.

3.2 *Boundary Element Simulations*

The results of the preceding section provide a framework for analyzing the characteristics of interface waves that propagate along a fracture. These results, however, do not completely address the more fundamental question of how to generate fracture interface waves from a source of finite size. In addition, the analysis does not provide information on the existence of other possible types of interface waves with displacement characteristics different from that assumed in Eq.(3) and (4).

To explore these questions, a dynamic boundary element code has been developed for modeling wave propagation in a medium containing fractures (Gu, 1994). The code is a time domain implementation of the dynamic Boundary Element Method (BEM) for multiple regions that are coupled together by the displacement-discontinuity boundary conditions given in Eq.(1) and (2). In this scheme, the upper and lower fracture surfaces are divided into quadratic boundary elements. The time integration is performed using an explicit time stepping algorithm. The displacement-discontinuity boundary conditions given in Eq.(1) and (2) are applied between the upper and lower fracture surfaces to form a system of linear equations for the displacements on the fracture. The surface displacements are directly obtained by solving the system of linear equations and the surface tractions are computed from these displacements using Eq.(1). The displacements at any point off of the fracture can be computed from the values on the fracture by numerically integrating the elastodynamic integral representation equation.

For the geometry shown in Fig.6, the results of the previous section suggest that the symmetric wave is best generated by a horizontally polarized source and the antisymmetric interface wave by a vertically polarized source, as displayed schematically in Fig.7. For a horizontal source centered on the fracture, the symmetry of the problem requires that the horizontal displacement on the upper and lower surfaces, u_x^a and u_x^b be equal, which through examination of Eq.(1), reveals that the symmetric wave is independent of the tangential component of fracture stiffness. Similarly, the problem symmetry for a vertical source centered on the fracture requires that the antisymmetric wave be independent of the normal component of the fracture stiffness.

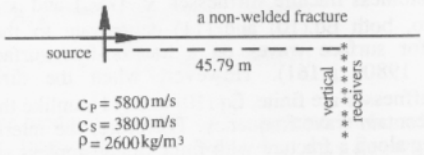

Figure 6. Two dimensional boundary element simulation geometry illustrating (line) source location and orientations (arrows) used to generate symmetric and antisymmetric interface waves.

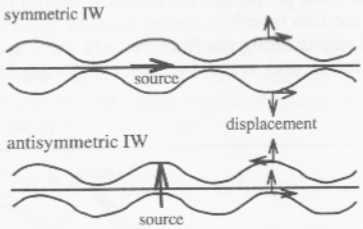

Figure 7. Schematic view of symmetric and antisymmetric interface waves.

In the numerical experiments, the rock surrounding the fracture is assigned P- and S-wave velocities c_P= 5800 m/s and c_S= 3800 m/s and a density ρ=2600 kg/m^3. A three-lobed wavelet with a central frequency of 800 Hz was used as the source wavelet. Fig.8 displays two seismic sections recorded on the lower fracture surface for horizontal and vertical line sources centered on a fracture with normal and tangential stiffnesses of $\kappa_x, \kappa_z = 5\times10^9$ Pa/m. Four arrivals are observed for both source orientations and are identified with the superscripts *PIW* to denote the P-type interface wave, *RIW* to denote a generalized Rayleigh interface wave, *P+PIW* to denote a mixture of a P-body wave and the P-type interface wave, and *S+RIW* to denote to a mixture of an S-body wave and a generalized Rayleigh interface wave. Clearly, if the fracture is completely welded, a receiver located at some horizontal distance on the fracture will observe only a P-wave from a horizontally polarized source and only an S-wave from a vertically polarized source. Thus the *PIW* and *RIW* arrivals detected on the vertical component for the horizontal source case and on the horizontal component are wave phenomena resulting from the finite fracture stiffnesses.

The *PIW* interface wave is generated by both the horizontally and vertically polarized sources and its, therefore, unlikely that this wave is the leaky symmetric interface wave described in the previous section (Fig.3). At present, it is postulated that this wave may be a leaky mode of the type described by Gilbert et al. (1962) for a traction-free surface. Since the amplitude of the *PIW* wave is sensitive to the fracture stiffnesses (Fig.9), this wave may also

a) horizontal source

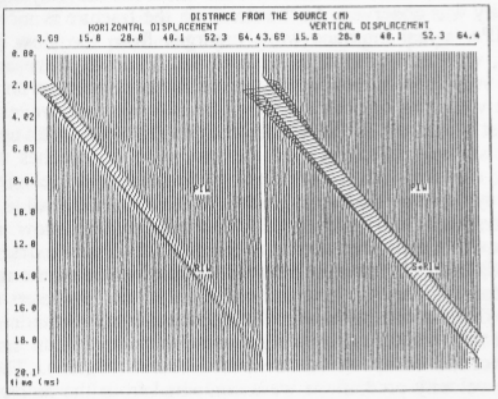

b) vertical source

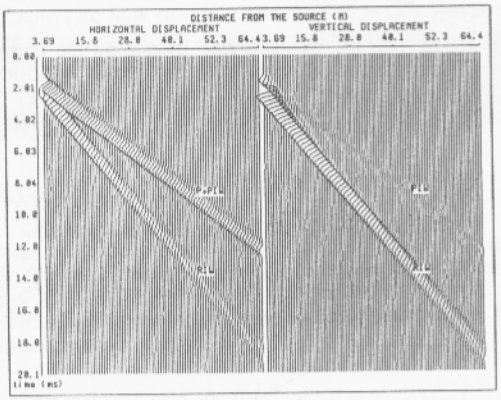

Figure 8. Seismic sections recorded along the lower surface of the fracture for sources oriented in the horizontal (a) and vertical (b) directions (Fig.6).

a) horizontal source

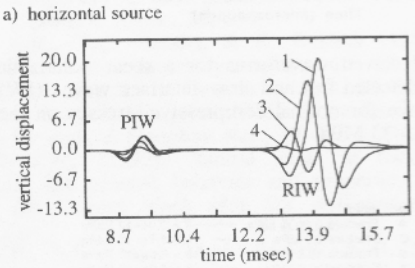

b) vertical source

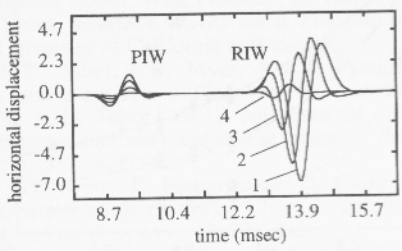

Figure 9. Waveforms recorded on the lower surface of a fracture 45.79 m from a source (Fig.6). Fracture stiffnesses for the horizontal source case are κ_z = (1) 1×10^9, (2) 5×10^9, (3) 2.5×10^{10} and (4) 1×10^{11} Pa/m, and for the vertical source case are κ_x = (1) 5×10^9, (2) 1×10^{10}, (3) 2.5×10^{10} and (4) 1×10^{11} Pa/m.

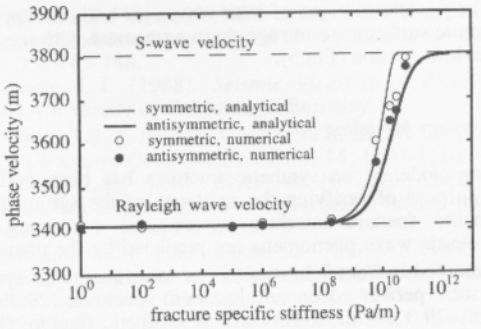

Figure 10. Phase velocities of *RIW* interface waves as a function of fracture specific stiffness for the geometry shown in Fig.6.

prove useful for remotely characterizing fracture properties provided that a theoretical understanding of this wave is developed.

To examine the effects of fracture stiffness on the interface waves, displacement traces recorded on the lower fracture surface 45.79 m from the source are displayed in Figure 9 for a range of fracture stiffnesses. Both the phase and amplitude of the waveforms vary with fracture stiffness. The phase velocities of the *RIW* interface waves obtained from numerical simulations are displayed in Fig.10 for a range of fracture stiffnesess, along with theoretical values computed from Eq.(10) and (11). Phase velocities obtained from the numerical simulation are in good agreement with the theoretical values for the symmetric and antisymmetric interface waves indicating that the *RIW* arrivals are indeed generalized Rayleigh interface waves.

The particle motions of the symmetric and antisymmetric interface waves computed on the upper and lower fracture surfaces 45.79 m from the source for the geometry of Fig.6 are displayed in Fig.11 for $\kappa_x, \kappa_z = 5\times10^9$ Pa/m. The symmetric wave is generated by a horizontal source and the antisymmetric wave by a vertical

a) symmetric interface wave

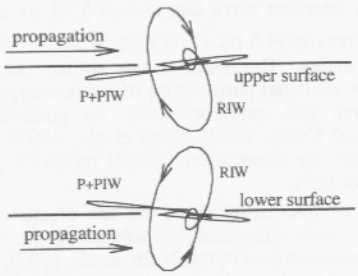

b) antisymmetric interface wave

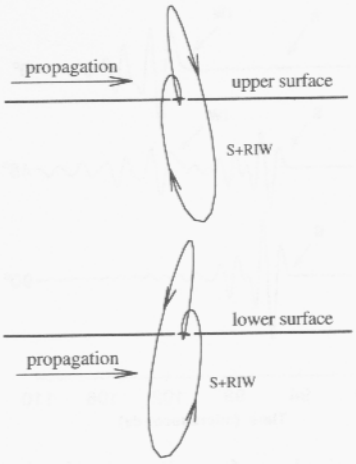

Figure 11. Particle motions on the upper and lower surfaces of a fracture 45.79 m from the source for the geometry of Fig.6.

interface wave for stiffnesses ranging from $4x10^{12}$ to $3x10^{13}$ Pa/m are in good agreement with the experimental data. These results indicate that it is possible to generate an antisymmetric interface wave of the from predicted by Eq.(11) using a polarized shear source oriented perpendicular (0° degrees) to the fracture.

4 SUMMARY AND CONCLUSIONS

Despite having negligible thickness, fractures in rock represent compliant interfaces that are capable of supporting a class of elastic interface waves. Plane wave analysis of a fracture embedded in an elastic medium produced two distinct fracture interface dispersion equations with mathematical forms similar to the classic free-surface Rayleigh wave equation. Analysis of these equations revealed that both waves are dispersive and that each wave depends on either the normal or shear fracture stiffness. Laboratory experiments on artificial fractures and numerical simulations performed with the dynamic boundary element method confirmed the existence of the two fracture interface waves. Numerical simulations also predict a fast compressional interface wave. We are presently exploring the properties of this wave and determining whether it can be observed in the laboratory. The results of this study demonstrate how to excite and detect interface waves which propagate on single fractures using polarized sources and how to use measured velocities of these waves to extract the fracture stiffnesses. Future work will focus on analyzing the partitioning of energy between body waves and interface waves and the effects of multiple fractures.

ACKNOWLEDGEMENTS

This work was supported by the Director, Office of Energy Research, Office of Basic Energy Sciences under U.S. Department of Energy Contract No. DE-AC03-76SF00098 and DE-F602-93ER14391. LJPN would also like to acknowledge the Young Investigator award of the NSF.

REFERENCES

Aki, K. & P.G. Richards (1980). *Quantitative Seismology*, vol. I, W.H. Freeman & Co., New York.

Angel, Y.C. & J.D. Achenbach (1985). Reflection and transmission of elastic waves by a periodic array of cracks, *J. Appl. Mech.*, 52, 33-41.

Bandis, S.C., A.C. Lumsden, & N.R. Barton (1983). Fundamentals of rock joint deformation, *Int. J. Rock Mech. Min. Sci. & Geomech. Abstr.*, 20, 249.

Barton, N.R., S.C. Bandis, & K. Bakhtar (1985). Strength, deformation and conductivity coupling of rock joints, *Int. J. Rock Mech. Min. Sci. & Geomech. Abstr.*, 22, 121.

Cook, N.G.W. & K. Hodgson (1965). Some detailed stress-strain curves for rock, *J. Geophys. Res.*, 70, 2883-2888.

Cook, N.G.W. (1992). Natural joints in rock: mechanical, hydraulic and seismic behavior and properties under normal stress, *Int. J. Rock Mech. Min. Sci. & Geomech. Abstr.*, 29, 198-223.

Gilbert, F., S.J. Laster, M.M. Backus, & R. Schell (1962). Observations of pulses on an interface, Bull. Seism. Soc. Am., 52, 847-868.

Goodman, R.E. (1976). *Methods of Geological Engineering in Discontinuous Rocks*, West Pub. Co., St. Paul.

Gu, B. (1994). *Interface Waves on a Fracture in Rock*, PhD Thesis, University of California at Berkeley.

Gu, B., K.T. Nihei, L.R. Myer, & L.J. Pyrak-Nolte (1995). Fracture interface waves, *J. Geophys. Res.* (submitted).

Kendall, K. & D. Tabor (1971). An ultrasonic study of area of contact between stationary and sliding surfaces, *Proc. Roy. Soc. London*, A, 323, 321-340.

Morlet, J., G. Arens, E. Fourgeau, & D. Giard (1982). Wave propagation and sampling theory - part II: sampling theory and complex waves, *Geophys.*, 47, 222-236.

Myer, L.R. & E.L. Majer (1984). Evaluation of technology for detection of anomalies during repository excavation at the BWIP site, Basalt Waste Isolation Project, Hanford, WA, SD-BWI-TI-262.

Nagy, P.B., D.V. Rypien, & L. Adler (1990). Dispersive properties of leaky interface waves in adhesive layers, in *Review of Progress in Quantitative Nondestructive Evaluation*, D.O. Thompson and D.E. Chimenti (eds), 9, 1247-1254.

Nihei, K.T., L.R. Myer, N.G.W. Cook & W. Yi (1994). Effects of non-welded interfaces on guided SH-waves, *Geophys. Res. Lett.*, 21, 745-748.

Pyrak-Nolte, L.J. (1988). *Seismic Visibility of Fractures*, PhD Thesis, University of California at Berkeley.

Pyrak-Nolte, L.J. & N.G.W. Cook (1987). Elastic interface waves along a fracture, *Geophys. Res. Lett.*, 14, 1107-1110.

Pyrak-Nolte, L.J., L.R. Myer, & N.G.W. Cook (1990a). Transmission of seismic waves across single natural fractures, *J. Geophys. Res.*, 95, 8617-8638.

Pyrak-Nolte, L.J., L.R. Myer, & N.G.W. Cook (1990b). Anisotropy in seismic velocities and amplitudes from multiple parallel fractures, *J. Geophys. Res.*, 95, 11345-11358.

Pyrak-Nolte, L.J., J. Xu, & G.M. Haley (1992). Elastic interface waves propagating in a fracture, *Phys. Rev. Lett.*, 68, 3650-3653.

Pyrak-Nolte, L.J. & D.D. Nolte (1995). Wavelet analysis of velocity dispersion of elastic interface waves propagating along a fracture, *Geophys. Res. Lett.* (accepted).

Rokhlin, S.I. & Y.J. Wang (1991). Analysis of boundary conditions for elastic wave interaction with an interface between two solids, *J. Acoust. Soc. Am.*, 89,503-515.

Schoenberg, M. (1980). Elastic wave behavior across linear slip interfaces, *J. Acoust. Soc. Am.*, 68, 1516-1521.

Stoll, R.D. (1989). Stress-induced anisotropy in sediment acoustics, *J. Acoust. Soc. Am.*, 85, 702-708.

Suárez-Rivera, R. (1992). *The Influence of Thin Clay Layers Containing Liquids on the Propagation of Shear Waves*, PhD Thesis, University of California at Berkeley.

Walsh, J.B. (1965). The effect of cracks on the uniaxial elastic compression of rocks, *J. Geophys. Res.*, 70, 399-411.